Improving the redox response stability of ceria-zirconia nanocatalysts under harsh temperature conditions

Article

Improving the Redox Response Stability of Ceria-Zirconia Nanocatalysts under Harsh Temperature Conditions

Carolina Arias-Duque, Eva Bladt, Miguel Ángel Muñoz, Juan C. Hernandez-Garrido, Miguel A Cauqui, José M. Rodríguez-Izquierdo, Ginesa Blanco, Sara Bals, José J. Calvino, José A. Pérez-Omil, and Maria P Yeste

Chem. Mater., **Just Accepted Manuscript** • DOI: 10.1021/acs.chemmater.7b03336 • Publication Date (Web): 10 Oct 2017

Improving the Redox Response Stability of Ceria-Zirconia Nanocatalysts under Harsh Temperature Conditions.

Carolina Arias-Duque,[†,‡] Eva Bladt,[§] Miguel A. Muñoz,[†,‡] Juan C. Hernández-Garrido,[†,‡] Miguel A. Cauqui,[†,‡] José M. Rodríguez-Izquierdo,[†,‡] Ginesa Blanco,[†,‡] Sara Bals,[§] José J. Calvino,[†,‡,*] José A. Pérez-Omil,[†,‡] María P. Yeste[†,‡]

[†]Departamento de Ciencia de los Materiales e Ingeniería Metalúrgica y Química Inorgánica. Facultad de Ciencias. Universidad de Cádiz, Campus Rio San Pedro, Puerto Real, 11510-Cádiz, Spain

[‡]Instituto Universitario de Investigación en Microscopía Electrónica y Materiales (IMEYMAT). Facultad de Ciencias. Universidad de Cádiz. Campus Río San Pedro, Puerto Real, 11510-Cádiz, Spain

[§]EMAT, University of Antwerp, Groenenborgerlaan 171, B-2020 Antwerp, Belgium

ABSTRACT: By depositing ceria on the surface of Yttrium-Stabilized Zirconia (YSZ) nanocrystals and further activation under high temperature reducing conditions, a 13% mol. CeO_2/YSZ catalyst structured as subnanometer thick, pyrochlore-type, ceria-zirconia islands has been prepared. This nanostructured catalyst depicts not only high Oxygen Storage Capacity (OSC) values but, more importantly, an outstandingly stable redox response upon oxidation and reduction treatments at very high temperatures, above 1000ºC. This behavior largely improves that observed on conventional ceria-zirconia solid solutions, not only of the same composition but also of those with much higher molar cerium contents. Advanced Scanning Transmission Electron Microscopy (STEM-XEDS) studies have revealed as key not only to detect the actual state of the lanthanide in this novel nanocatalyst but also to rationalize its unusual resistance to redox deactivation at very high temperatures. In particular, High Resolution X-Ray Dispersive Energy studies have revealed the presence of unique bilayer ceria islands on top of the surface of YSZ nanocrystals which remain at surface positions upon oxidation and reduction treatments up to 1000ºC. Diffusion of ceria into the bulk of these crystallites upon oxidation at 1100ºC irreversibly deteriorates both the reducibility and OSC of this nanostructured catalyst.

It is widely accepted that the introduction of Zr^{4+} in the crystal lattice of CeO_2 increases the reducibility and oxygen storage capacity (OSC), as well as the thermal stability and electrical conductivity of the fluorite structure, thus making ceria-zirconia mixed oxides excellent materials for a wide range of applications.[1-2] In fact, these oxides represent the state-of-the art of OSC materials for TWCs (three-way catalysts).[3] They have also been extensively investigated as catalysts and catalyst supports of noble metal nanoparticles for a variety of chemical processes related to the production of hydrogen for fuel cells (reforming, methane partial oxidation, CO oxidation, PROX, low temperature water gas shift, among others) or even as a component (cathode, anode or electrolyte) in solid oxide fuel cells (SOFC) fabrication.[4] After proper selection of the synthesis methods (including thermochemical treatments of the as-prepared samples), the chemical composition is a critical aspect to determine OSC, considered as a key descriptor of the catalytic performance of ceria-zirconia materials in the aforementioned applications.[5] Thus, in a theoretical DFT study about the influence of composition on the redox properties of these mixed oxides, Wang et al. conclude that a Ce/Zr ratio close to unity is a requisite for $Ce_{1-x}Zr_xO_2$ solid solutions to depict outstanding OSC properties.[6] However, recent reports published by different national agencies and expert working groups on defining critical raw materials and strategies to cope with their supply risks have clearly recommended a reduction in the usage of rare-earth materials in current technologies.[7] Taking this fact into account, it seems reasonable that optimizing the total amount of ceria in ceria-based formulations arises as an issue of great interest in the fields of heterogeneous catalysis and fuel cell fabrication.[8-9] At least two strategies can be pursued to reach this optimization goal. On one hand, it is clear that limiting the total amount of the lanthanide in the preparation of the mixed oxide would contribute to a more limited usage whenever the prepared materials provide the same or, even better, improved, performance on a per unit mass base. Likewise, extending the lifetime of the materials in the application of interest appears as an interesting alternative.

The last approach connects with stability under working conditions, which is one of the major concerns in the design of improved formulations of TWC components. In fact, increasingly stringent regulations, requiring lower emission standards, have lead to higher temperature of emissions,[10] which promote faster deactivation of the TWC components, particularly in terms of OSC.[11]

A variety of strategies have been assayed to improve stability under high temperature working conditions, including: (1) the use of modified synthesis procedures of the CeO_2-ZrO_2 mixed oxide;[12] (2) mixing at the nanoscale to prepare composites both of ceria-zirconia/alumina [10, 13-15] and of ceria-zirconia with two different compositions [16] or (3) doping the mixed

oxide with other metallic elements.[17-18] In the case of nanocomposites with alumina, the underlying stabilization concept is that of creating a diffusion barrier [19] between neighboring mixed oxide particles, which allows for maintaining dispersion and OSC.

Anchoring isolated ceria-zirconia nanostructures onto the surface of a carrier material, by supporting them onto a support, constitutes an alternative way of implementing this diffusion barrier concept, as long as diffusion at high temperature into the bulk of the carrier material is actually limited. In fact supported ceria [20] and ceria–zirconia [21-22] have been reported to be highly resistant to sintering under reduction–oxidation treatments.

In this context, the question arises whether materials with low total cerium content, high reducibility and OSC as well as high stability under high temperature conditions can be prepared.

Kaspar et al. reported on a $Ce_{0.2}Zr_{0.8}O_2$ oxide, synthesized by coprecipitation, which showed good OSC and reducibility at low temperatures.[23] Nevertheless, the stability of the redox properties of these oxides upon high-temperature oxidation treatments (>900ºC) was not investigated by the authors.

Likewise, in a previous paper, we reported on a new family of ceria-yttria-stabilized zirconia oxides (CYSZ), with low Ce content (<20%) exhibiting very high OSC values and outstanding reducibility at very low temperature (150ºC).[22] The strategy to prepare this material relied on depositing ceria on the surface of yttria-doped zirconia (YSZ) nanocrystals and benefiting from the structural and chemical interactions that can be established between ceria and zirconia after proper high temperature redox treatments.[6, 24-29] We showed that the redox functionality of this CYSZ catalyst was highly dependent on the thermochemical history of the sample, particularly on the application of high temperature treatments.

Thus, a CYSZ catalyst depicting optimum redox properties was obtained after three consecutive reducing-oxidizing cycles, where reduction steps were performed under H_2/Ar, at 950ºC (1h) (Severe Reduction or SR) and followed by oxidation under O_2/He, either at 500ºC (1h) (Mild Oxidation or MO) or 950ºC (Severe Oxidation or SO). The singular redox properties exhibited by the CYSZ-SRMO-SRSO-SRMO catalyst were associated to the formation of sub-nanometer thick $Ce_2Zr_2O_7$ pyrochlore structures at the surface of the YSZ particles during the reduction treatment, which were transformed into $Ce_2Zr_2O_8$ during the MO steps.[22]

In this contribution we focus now on studying the stability of the redox response, in terms of both reducibility and OSC, of this promising material under high temperature aging treatments consisting of reduction-oxidation cycles at increasing temperatures. Results evidence a high resistance and reversibility of the redox behavior, which starts only to decay after prolonged (10h) oxidizing treatments at 1100ºC. Moreover, such high resistance has been fruitfully correlated with analytical studies, performed at atomic scale using state-of-the-art aberration-corrected equipment, which provide evidences of the limitation of diffusion of Cerium species into the bulk of the catalyst nanoparticles.

EXPERIMENTAL

The material used as support, YSZ (99.961% pure, S_{BET} 89 m^2 g^{-1}) with 15% molar of Y, was supplied by Tecnan-Nanomat S.L. A 13% mol CeO_2/YSZ catalyst was prepared by incipient wetness impregnation of the YSZ oxide (25 g), in three successive steps, using an aqueous solution of $Ce(NO_3)_3.6H_2O$ (1.2 M). After impregnation, the sample was dried in air, in an oven, overnight at 110ºC and further calcined, also under air, at 500ºC for 1 h. the specific surface area of the supported catalysts was 73 m^2 g^{-1}.

To obtain the material with optimum redox properties, this as-prepared CYSZ catalyst was sequentially submitted to the following three redox-aging steps:

(1) SRMO, Severe Reduction (SR) followed by Mild Oxidation (MO) treatment, consisting of: heating under a flow of H_2(5%)/Ar (60 cm^3 min^{-1}) from room temperature up to 950ºC, at a heating rate of 10 ºC min^{-1} and followed by 2 h of isothermal treatment at 950ºC. Next, the gas flow was switched to He (60 cm^3 min^{-1}), for 1 h, and the sample was cooled down to 25ºC under inert gas flow (60 cm^3 min^{-1}). After this severe reduction (SR) step, the aging cycle was closed by applying a mild re-oxidation, MO, routine. To prevent overheating of the reduced mixed oxides, this part of the cycle started with a re-oxidization at 25ºC, by pulsing an O_2(5%)/He mixture until there was no evidence of further oxygen consumption. The sample was then heated in a flow of O_2(5%)/He (60 cm^3 min^{-1}) up to 500ºC, the temperature at which the oxidation treatment was prolonged for 1 h. Finally, the sample is cooled down under the same atmosphere to room temperature.

(2) SRMO-SRSO: the as-prepared catalysts were first submitted to a SRMO treatment. Then a second SR treatment is applied. The redox cycle is closed by a Severe Oxidation, SO, treatment. This SO step included the room temperature pulse re-oxidation using O_2(5%)/He, and further ramp and isothermal heating under the same atmosphere but up to a final temperature of 950ºC, which was maintained during 1h.

(3) SRMO-SRSO-SRMO: in this case portions of the initial as prepared catalysts were successively submitted to first a SRMO cycle, then to a SRSO one and, finally, to a second SRMO treatment.

A pictorial description of all these treatments has been included in Figure S1 of supporting information.

This CYSZ-SRMO-SRSO-SRMO catalyst, which features optimum OSC and reducibility under H_2, is the starting point in all the deactivation studies under oxidizing conditions at high temperature investigated in this work. For the sake of brevity, it will be referred in the following as CYSZ-3C. The deactivation studies consisted of heating under O_2(5%)/He to a final temperature of 950ºC, 1000ºC or 1100ºC during 10h.

A conventional $Ce_{0.15}Zr_{0.85}O_2$ mixed oxide, in which Ce is distributed at bulk level and used as a reference (S_{BET} 40 m^2g^{-1}), was provided by Rhodia.

Textural properties of the samples were determined by N_2 adsorption at -196 ºC using a Quantachrome Autosorb iQ automatic device. Before measurement, samples were pre-evacuated at 200ºC for 2 h.

Inductively coupled plasma-atomic emission spectrometry (ICP-AES) was employed to determine the Ce loadings of the catalysts. X-ray diffraction (XRD) analyses of the catalysts were carried out using a Bruker diffractometer Model D8 ADVANCE operated at 40 kV and 40 mA employing Cu Kα radiation.

TPR-MS studies were performed in an experimental device coupled to a Pfeiffer, model Thermostar QME-200-D-35614, quadrupole mass spectrometer using 200 mg of sample, a 5% H_2/Ar flow rate of 60 cm^3 min^{-1} and a heating ramp of 10 ºC min^{-1}. Prior to all the H_2-TPR runs, the samples were cleaned by heating up to 500ºC under 5% O_2/He flowing at 60 cm^3 min^{-1}, at a heating rate of 10 ºC min^{-1}; then, they were kept for 1 h at this temperature and further cooled down to 150ºC under the flow of diluted oxygen and finally to 25ºC in He. The results are presented in the form of water evolution (mass/charge ratio=18) *vs* temperature, during the reduction process. Consistency with hydrogen consumption profiles was in all cases confirmed.

Ultimate OSC values were obtained from oxygen volumetric chemisorption experiments. The isotherms were recorded at 200ºC on a Micromeritics ASAP 2020 instrument in the oxygen partial pressure interval 0–300 Torr. The samples (400 mg) were pre-reduced by heating in a flow of 5% H_2/Ar (60 cm^3 min^{-1}) at 10 ºC min^{-1}, from 25ºC up to the selected reduction temperature (T_{redn}); they were kept at T_{redn} for 1 h under flowing 5% H_2/Ar; then they were evacuated for 1 h (residual pressure < 1.10^{-6} Torr at T_{redn} or 500ºC if T_{redn} was lower than 500ºC) and were finally cooled down to 200ºC under high vacuum. These evacuation conditions ensure the elimination of any significant amount of hydrogen chemisorbed on the oxides.

Samples for TEM/STEM analysis were obtained by dissolving the nanocrystal powder in ethanol and dropcasting the solution onto carbon-coated TEM grids at room temperature. TEM/STEM characterization was performed using different microscopes. A JEOL2010F microscope (not aberration corrected) equipped with a Field Emission Gun, a 80 mm^2 Oxford X-Max SDD detector for XEDS analysis was used to record HRTEM, HAADF-STEM and STEM-XEDS at resolutions above the angstrom level. Aberration-Corrected High Resolution STEM (HR-STEM) images were acquired using a FEI Titan^3 microscope operated at 300 kV. A semi convergence angle of ~21 mrad was used together with a camera length of 115 mm. Energy Dispersive X-ray Spectroscopy (XEDS) measurements with a resolution at the nanometer scale were performed using a FEI Tecnai G2 electron microscope operated at 200 kV. X-EDS experiments at the atomic scale were carried out using an aberration corrected FEI Titan^3 microscope operated at 300 kV and equipped with a ChemiSTEM system.[30] Analysis was performed using the Bruker ESPRIT software.

X-ray Photoelectron Spectra were obtained using a Kratos Axis Ultra DLD instrument, and recorded with monochromatic Al Kα radiation (1486.6 eV). The instrument was operated in the fixed analysis transmission mode (FAT), using pass energy of 20 eV. The Kratos coaxial charge neutralization system was used to compensate charging effects, and the binding energy scale was calibrated with respect to Zr 3d5/2 component at 182.64 eV.[31] The spectrometer was connected to a catalytic cell which allowed the reduction of samples and their anaerobic transfer to the analysis chamber.

RESULTS AND DISCUSSION

The main focus of the present study was determining the actual stability of the CYSZ-3C catalyst against redox cycling at high temperatures. To this purpose, it was submitted to an additional reducing-oxidizing cycle in which the reducing part of the cycle was again performed at 900ºC, but the final oxidation temperature was either increased above 950ºC, up to 1100ºC or prolonged in time (10h) at 950ºC. In the following, we will describe changes in the textural, redox and structural properties of the catalyst after these treatments. Concerning redox properties both reducibility under H_2 and OSC have been followed to monitor deactivation. Regarding structure, the macroscopic and atomic scale details have been tracked by combining XRD and TEM/STEM analysis in aberration-corrected equipment, respectively. Likewise, compositional changes at the surface (XPS) as well as at nanometer and atomic scale have been monitored through STEM-XEDS measurements.

Texture: Surface Area

Concerning textural properties, Table 1 gathers the BET surface area values of the different materials. Note that the preparation of the CYSZ-3C catalyst involves a large drop of surface area, from 70 in CYSZ down to 22 m^2 g^{-1}, in spite of what the redox properties improve significantly. Note that the application of an additional SRSO cycle in which oxidation is performed at 950ºC during 1h, does not affect the surface area. At this temperature, oxidation has to be prolonged for 10h to decrease further the surface area (17 m^2 g^{-1}). Nevertheless the largest drop takes place when oxidation is performed at 1100ºC, after which the surface area is negligible, 1 m^2 g^{-1}.

Table 1. BET surface area values.

SAMPLE	S_{BET} (m^2 g^{-1})
CYSZ	73
CYSZ-3C	22
CYSZ-3C SRSO (950ºC 1h)	26
CYSZ-3C SRSO (950ºC 10h)	17
CYSZ-3C SRSO (1000ºC 10h)	13
CYSZ-3C SRSO (1100ºC 10h)	1
$Ce_{0.15}Zr_{0.85}O_2$	40
$Ce_{0.15}Zr_{0.85}O_2$ SRMO-SRSO	37

In terms of texture, the reference bulk catalyst with similar composition, $Ce_{0.15}Zr_{0.85}O_2$, retains better its surface area. Thus, after the SRMO-SRSO 950 (1h) cycle it only drops from 40 down to 37 m^2 g^{-1}. It will be important to take into account this fact when we compare later the redox performance of this catalyst with that of CYSZ-3C.

Redox Behavior

Concerning changes in reducibility it pertains to recall first, for a more comprehensive understanding, the changes taking place during the preparation of the CYSZ-3C catalyst. Thus Figure 1, collects the H_2-TPR diagrams obtained on the CYSZ catalyst as prepared, plot 1(a), after a first SRMO treatment, plot 1(b), and, finally after the complete SRMO-SRSO-SRMO treatment, i.e thereafter labeled as CYSZ-3C, plot 1(c). Note how the evolution of water, which corresponds to oxygen abstraction from the sample by H_2, changes dramatically after the first SRMO treatment. Thus from an evolution in a wide

temperature window located at intermediate-high temperature values (400-800ºC) in the CYSZ sample, it changes to, mostly, a major peak at roughly 250ºC which is followed by a tail and a secondary, minor, peak at 500ºC. Still a further improvement in reducibility is observed in the CYSZ-3C oxide, whose H_2-TPR diagram shows only an intense peak at roughly ~220ºC, tailing asymmetrically towards the high temperature end. This redox behavior contrasts with that of the bulk oxide, whose H_2-TPR diagram after an SRMO-SRSO-SRMO treatment, plot 1(f), does not differ two much from that of the original, untreated sample, plot 1(d), and/or SRMO treated one, plot 1(e). In the cycled bulk oxide reduction takes place in the middle-high temperature range, peaking at 500ºC.

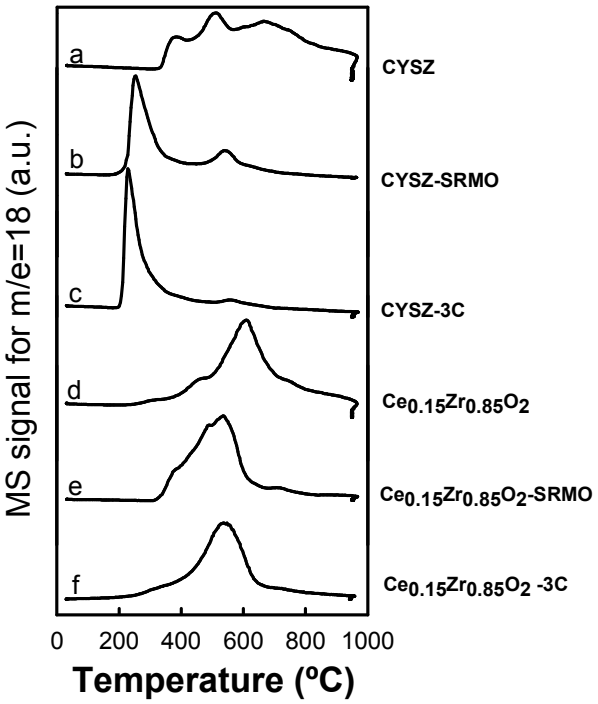

Figure 1. H_2-TPR diagrams for the CYSZ and $Ce_{0.15}Zr_{0.85}O_2$ oxides submitted to different aging treatments.

The effect of the SRSO cycles under stringent conditions on the CYSZ-3C material is illustrated in Figure 2. The reference H_2-TPR in this case is, of course, that of CYSZ-3C, plot 2(a). Thus, when the SRSO treatment is applied at 950ºC for 1h, the reducibility changes dramatically, the H_2-TRP diagram showing now only a very narrow peak centered at about 500ºC, plot 2(b), which suggests the formation of a very well-defined phase, whose oxygen is much more tightly bonded to the mixed oxide than in the CYSZ-3C sample. This low-reducibility state can nevertheless transform reversibly back into the initial high-reducibility one by a further SRMO treatment, plot 2(c).

When the SRSO treatment at 950ºC is extended for 10h the result resembles that described previously, plot 2(d). Again the reducibility worsens after oxidation at high temperature. In this case, a wider oxidation peak centered at about 400ºC is observed.

An increase of the SRSO final temperature up to 1000ºC, for 10h, results once more in a thin reduction peak at 500ºC, plot 2(e), which transforms back into a low temperature peaking profile upon SRMO treatment, plot 2(f). Therefore, the reversibility to an optimum redox response is still maintained after such severe oxidation.

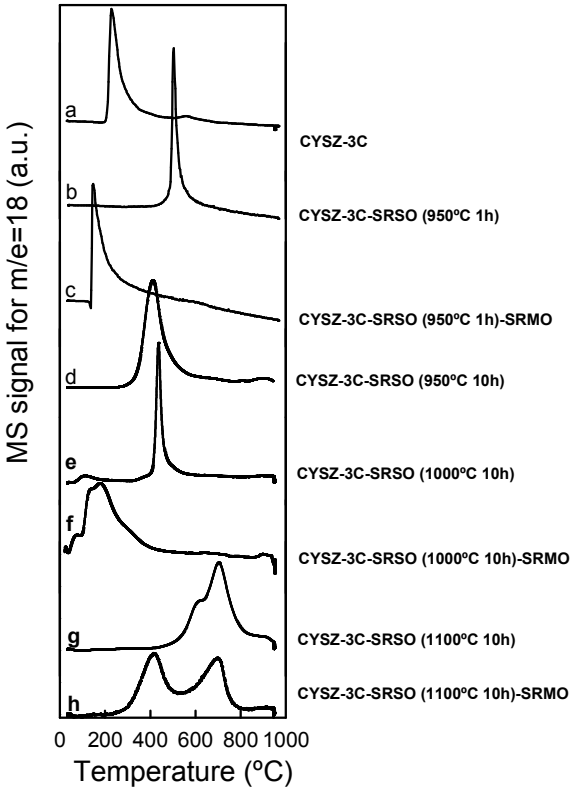

Figure 2. H_2-TPR diagrams for the CYSZ-3C material submitted to SRSO cycles under stringent conditions.

Nevertheless, when the SRSO treatment is performed at 1100ºC this reversibility is definitely lost. The reduction events in the H_2-TPR diagram appear now at much higher temperatures, in the 500-800ºC range, in the form of two overlapped and broad peaks, plot 2(g). Moreover, when an additional SRMO treatment is applied to this state, plot 2(h), two broad peaks appear; the first one locates at much higher temperature than in previous cases, with maximum at 400ºC, and the second resembles the situation in the SRSO-1100ºC sample. This evidence only a partial recovery of reducibility but to a state neatly different from that prevailing in all the SRMO samples commented up to this point.

Summarizing the H_2-TPR results, the CYSZ-3C catalyst demonstrates a remarkable resilience in its low temperature reducibility when submitted to cyclic redox aging up to 1100ºC. This temperature marks a breakpoint above which redox response is irreversibly degraded, in terms of recovery of low temperature reducibility.

Ultimate OSC measurements allow establishing quantitative comparisons of reducibility at different temperatures among the whole set of samples. Figure 3 gathers OSC data measured after reduction at low (350ºC) and intermediate (500ºC) temperature. The results are presented as bar graphs to allow for a direct, visual, comparison. Numerical values, expressed both as μmol-O/g of catalyst and as percentage of Ce^{3+} can be found in Table S1 in Supporting Information.

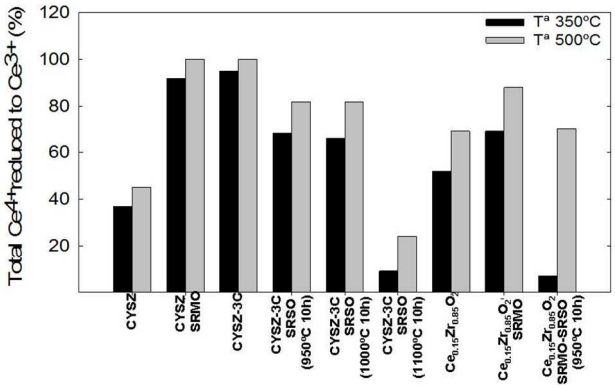

Figure 3. OSC values after reduction at 350ºC and 500ºC.

To a large extent, the H_2-TPR described above anticipate the OSC results gathered in this Figure. Starting with the comparison between the conventional, bulk type, $Ce_{0.15}Zr_{0.85}O_2$ and CYSZ-3C catalyst, it becomes clear that the latter exhibits higher OSC values, especially after reduction at low temperature. Only in the fresh state the bulk sample stores more oxygen. This latter result is not surprising since in the as-prepared state the supported CYSZ catalyst consists of CeO_2 nanostructures supported on the YSZ crystallites, whereas in the bulk sample ceria is already forming a mixed oxide with zirconia, which is well established to improve the redox behavior of pure ceria. This last observation can therefore be considered as indication that in the as-prepared CYSZ catalyst ceria and zirconia have not formed a mixed phase yet. Further characterization data support this interpretation.

Concerning the effect of redox treatments, it appears clear the benefiting effect of the initial SRMO protocol on both samples, but especially on the CYSZ catalyst, which exhibits full Ce reduction at 500ºC and a 92% Ce^{3+} content at 350ºC. The corresponding values in the bulk sample are just 73% and 29%. When a complete SRMO-SRSO-SRMO treatment is applied to the CYSZ catalysts, as observed by its H_2-TPR, the OSC values slightly enhanced now showing full Ce reduction at 500ºC and a 95% Ce^{3+} content at 350ºC.

After aging at 950ºC for 10h the OSC values of the CYSZ-3C catalyst are also above those of the bulk sample. Moreover, very large differences are observed in terms of storage at low temperature, 68% and just 7% for CYSZ-3C and $Ce_{0.15}Zr_{0.85}O_2$-SRMO-SRSO, respectively. This moderate aging treatment severely deteriorates the redox response of conventional bulk formulations but does affects only in a very limited extent to the CYSZ one. For this reason, further, much more severe aging treatments were only applied to CYSZ-3C. Note at this respect that increasing the temperature of the aging, oxidizing, treatment up to 1000ºC, also for 10h, does not affect the oxygen storage capacity of this material, which still presents Ce^{3+} contents close to 70 and 80% after reduction at 350 and 500ºC.

As already observed in the H_2-TPR traces, a dramatic change takes place when the aging process is applied at 1100ºC for 10h. After this treatment, OSC drops down to roughly 25% and 10% at 500 and 350ºC, respectively. Therefore, OSC measurements confirm that 1100ºC under oxygen are limiting working conditions for the CYSZ catalyst prepared in this work.

Structural Characterization

An in-depth characterization study was performed to understand the correlation of the redox behavior of the CYSZ catalyst with structural features. At macroscopic level, the corresponding XRD diagrams were recorded after the different redox aging treatments; Figure 4 and Table S2 gather the corresponding information. The diffraction peaks observed in the XRD diagram of the YSZ oxide used as support can be assigned to a tetragonal type oxide with the cell parameters shown in Table S2. A tetragonalization ratio (c/a) just 1% larger than that expected for the tetragonal description of the cubic fluorite cell (c/a=$\sqrt{2}$=1.414) is observed. Taking into account that, in terms of the unit cell parameters, the phase is quite close to a cubic one, we can index the reflections in reciprocal space either on the basis of the tetragonal cell or the "nearly-cubic" cell. The relationship between the axis of the two unit cell are the following: $\mathbf{a}_t=1/2(\mathbf{a}_c-\mathbf{b}_c)$, $\mathbf{b}_t=1/2(\mathbf{a}_c+\mathbf{b}_c)$, $\mathbf{c}_t=\mathbf{c}_c$, where "t" and "c" sub-indices refer to the tetragonal and cubic unit cells.

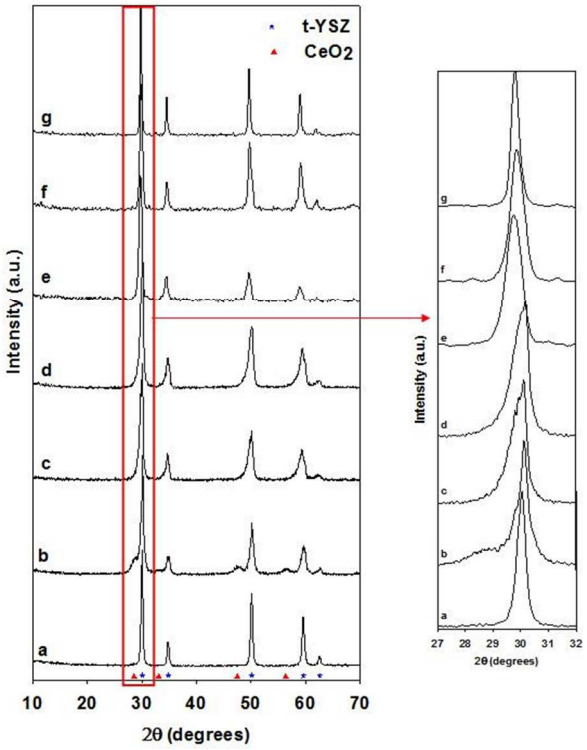

Figure 4. XRD diffractograms of the YSZ (**a**) and CYSZ samples submitted to different redox aging treatments: CYSZ (**b**), CYSZ-3C (**c**), CYSZ-3C-SRSO (950ºC 1h) (**d**), CYSZ-3C-SRSO (950ºC 10h) (**e**), CYSZ-3C-SRSO (1000ºC 10h) (**f**) and CYSZ-3C-SRSO (1100ºC 10h) (**g**)

Apart from subtle changes in position and narrowing, these peaks remain visible in the whole set of XRD diagrams, this indicating that the structure of the YSZ crystallites remain mostly unchanged. After deposition of ceria onto the surface, the peaks corresponding to this phase are clearly detected in the CYSZ as-prepared catalyst, in good agreement with the OSC results previously described. No change in the c/a ratio takes place either. After the SRMO-SRSO-SRMO treatment that leads to the CYSZ-3C material, these pure CeO_2 peaks are no longer visible, this clearly indicating mixing of this component with the YSZ support.

The enlargement of the 2Θ range corresponding to the {011} planes of the tetragonal phase, between 28-31º, shows an asymmetric peak tailing towards the low angle range. This would be consistent with the presence of a bulk, Zr-rich, YSZ phase and a surface type Ce-Zr phase.

The application of the high temperature redox aging treatments SRSO to the CYSZ-3C catalyst tend to erase this asymmetry, especially at the highest oxidation temperatures (>950ºC), this suggesting, as expected, that mixing between the two components of the catalyst increases with oxidation temperature. The peak becomes fully symmetric after oxidation at 1100ºC. In parallel, the (101) peaks become narrower, especially after the treatment at 1100ºC, which clearly correlates with the large drop in surface area after this severe treatment.

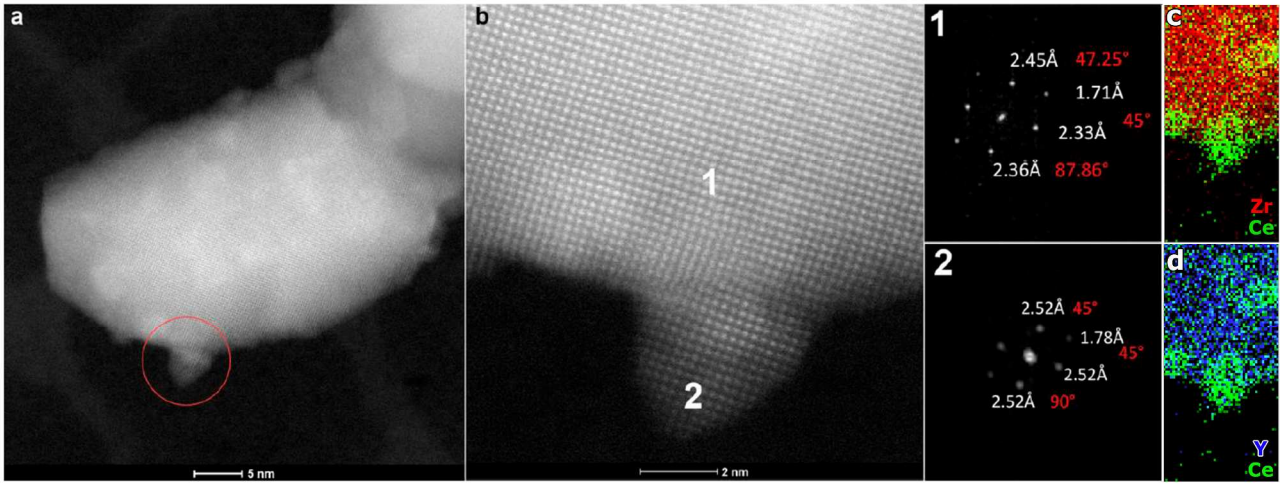

Figure 5. (a) HAADF-STEM image and (b) a more detailed high resolution STEM image of the starting CYSZ catalyst. Two regions are indicated in (b), showing *d*-spacings and angles allowing to index a YSZ region (1) and a CeO_2 fluorite-region (2). XEDS maps (c) and (d) show the presence of ceria nanoparticles (green) attached to the surface of an yttria-stabilized zirconia nanocrystal, in which zirconium is presented in red (c) and yttrium in blue (d).

The atomic scale structure of the CYSZ catalyst after the most relevant treatments was investigated by a combination of advanced STEM techniques. Figure 5, contains information representative of the structure of the starting CYSZ catalyst. Thus, Figure 5(a) shows a medium magnification HAADF-STEM image of CYSZ. A more detailed, high resolution view is presented in Figure 5(b). Since in this imaging mode the intensity scales both with the atomic number of the elements in the imaged area (with roughly a dependence of the type $Z^{1.8}$) and thickness, Figures 5(a) and (b) suggest that the deposition of ceria results in the formation of nanosized 3D particles on the surface of the YSZ nanocrystals. Those observed in this figure are only between 2-4 nm in diameter. Diffraction spots observed in the FFT taken from regions support (1) and the supported particles (2) agree, within experimental error, with those expected for YSZ and CeO_2. In any case, the presence of these cerium-containing nanoparticles was confirmed by energy dispersive X-ray spectroscopy (XEDS), Figures 5(c) and (d). The cerium signal is indicated in green in the XEDS map in Figure 5(c) and (d). From both maps, it is clear that the nanoparticles, made only of CeO_2, are attached onto the yttria-stabilized zirconia nanocrystal (Zr: red, Y: blue) surfaces.

The use of an yttria-stabilized zirconia as ceria support has been suggested because of their expected structural coherence, as both components have a cubic crystal lattice (21). Note at this respect how the 3D CeO_2 nanoparticles grow epitaxially on the YSZ support, as it can be confirmed through the aligned reflections in the FFTs coming from both areas in Figure 5. Thus, in Figure 5(b) it is clear that the $[001]_t$ structure visible in the YSZ support crystallite is coherently prolonged into the two CeO_2 particles observed on the edge of the YSZ crystallite, being quite difficult to establish an interface between the two regions of the material. This result confirms the hypothesized structural coherence between the two components of the CYSZ catalyst.

Images shown in Figure 5 evidence an additional key question that must be taken into account in the STEM characterization of this type of catalysts. This is the difficulty to detect the Ce-containing nanostructures on the HAADF-STEM images. In fact, given the close structural relationship between the two components, CeO_2 and YSZ, the discrimination of the 3D CeO_2 nanoparticles observed in Figure 5(b) can only be achieved on the basis of nanoanalytical data, as that shown in Figures 5(c) and (d). Without high resolution STEM-XEDS data the atomic scale analysis of this type of materials is out of reach.

After the SRMO-SRSO-SRMO treatment, which leads to CYSZ-3C, significant structural changes take place. Figure 6 shows representative HAADF-STEM images of this material.

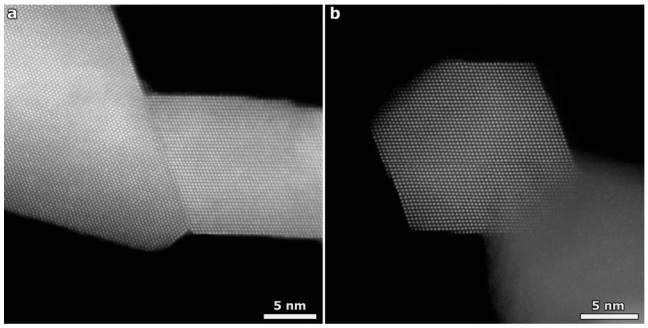

Figure 6. (a,b) High resolution HAADF-STEM images of CYSZ-3C nanocrystals.

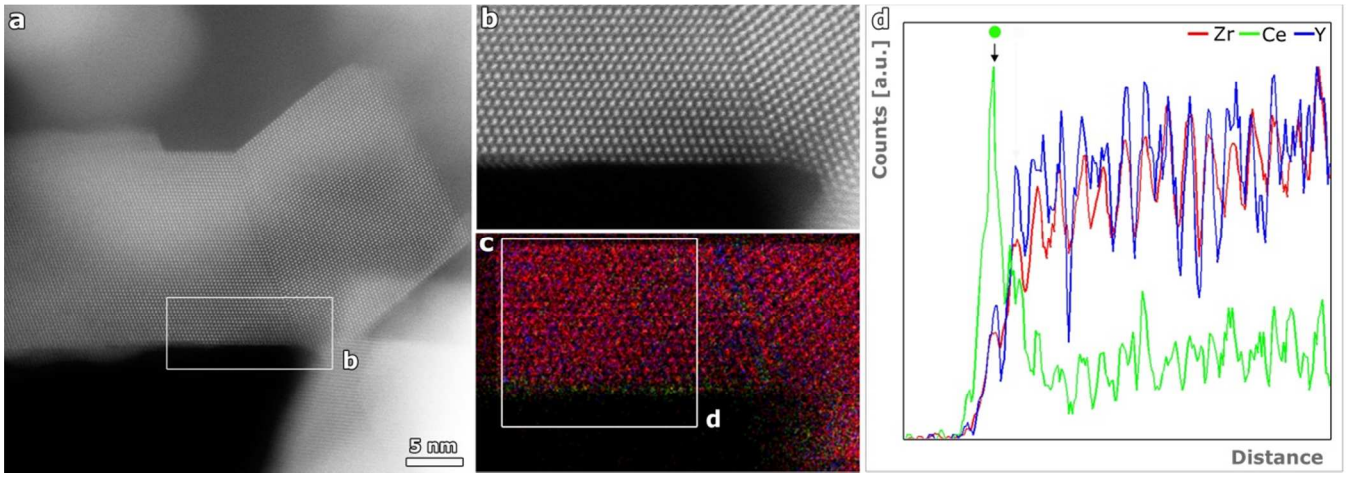

Figure 7. (a) High resolution HAADF-STEM image of a CYSZ-3C nanocrystal, where (b) indicates the area where XEDS maps were recorded; (c) Averaged X-EDS maps of Zr, Ce and Y; (d) line profile along the perpendicular to the edge of the CYSZ-3C nanocrystal.

Note how extended, flat, surfaces are now observed in the support. The crystallites are imaged along the [100] zone axis of the tetragonal YSZ unit cell, which corresponds to the [110] zone axis of the fluorite-type cubic unit cell. The edges of the images correspond to {011} tetragonal, {111} cubic, planes. Previous HAADF-STEM electron tomography experiments have evidenced[27, 32] that SRMO treatments lead to ceria-zirconia crystallites in which $\{111\}_c$ type surfaces represent the major contribution to their exposed area. This seems to be also the case in the YSZ support.

Note also that now there is no evidence of 3D, nanoparticle-like, structures. Moreover, there is no direct evidence about the location of Ce atoms. The image contrasts are rather uniform all over the areas occupied by the crystallites, from bulk to surface positions. In this case, only direct chemical analysis at the atomic scale is able to reveal the actual spatial distribution of Ce in CYSZ-3C, Figure 6.

Thus, Figure 7(a) shows a HAADF-STEM image of one of the crystallites along $[100]_t$. The STEM-XEDS map shown in Figure 6(c) was acquired in the area boxed in (a) and shown as enlargement in Figure 7(b). Note the atomic resolution achieved in the analytical map, which suggests at first sight a uniform distribution of Ce (green), Y (red) and Zr (blue) dots all over the imaged area. Nevertheless, intensity profiles of these three chemical signals along a line perpendicular to the $\{111\}_c$ surface lying horizontally, Figure 7(d) clearly reveals the details of the distribution of these elements. It is important to highlight at this respect that the Ce signal is very intense just at the position of the first plane at the very surface of the CYSZ-3C crystallite. A second atomic plane containing Ce, but in a lower amount, is observed. More to the interior of the crystallite, Ce is also observed but in lower amounts. Zr and Y signals are less intense at the first planes at the surface and then steadily increase from the third atomic plane on. A few remarks are worth being further commented with respect to these results.

First, it seems even clearer now, the absolute need of using advanced analytical tools, with atomic-scale resolution, to reveal the structure of this type of materials. To an extent, atomic resolution HAADF-STEM images are "blind" to the distribution of Ce in this particular type of nanostructures, in spite of the difference in atomic number values between Zr (Z=40), Y (Z=39) and Ce (Z=58). The intensity profiles of Zr and Y suggest a steep crystal thickness increase along the normal to the surface. Such thickness variation, which is in fact expected for the type of crystals detected after SRMO treatments in ceria-zirconia based materials, could compensate for the difference in atomic number between Ce and Zr-Y and, therefore, render the intensity of the atomic columns at the surface enriched in Ce similar to that of the Zr-Y columns at the bulk of the YSZ crystallites.

Second, it becomes clear that Ce concentrates at the very 1-2 first atomic planes at the surface of the material. This means that Ce atoms in the CYSZ-3C catalyst are at purely surface or subsurface positions. The first atomic plane is richer in Ce than in Zr or Y and the second one depicts a slightly larger concentration of the latter. In [22] the analysis at nanometer scale of this material showed islands with Ce/Zr ratios close to 1, which is compatible with the much more detailed, atomic scale, data presented in Figure 6. Finally, since the Ce signal does not fall to zero at bulk positions, an extended coverage of the YSZ crystallites is expected.

Third, Ce wets better the surface of YSZ after this treatment and adopts the form of flat extended nanostructures grown, as evidenced by the comparison between HAADF-STEM and STEM-XEDS data, epitaxially onto the YSZ support. Therefore, it seems that the textural change taking place in the support, which increases exposure of $\{011\}_t$ type facets ($\{111\}_c$), promotes a morphological change of the 3D islands observed in the starting CYSZ catalyst into this flat, subnanometer thick, unique nanostructures. Similar bilayers have already been detected in CeO_2/MgO catalysts after reduction at high temperatures,[20] though in that case HAADF-STEM images were enough to reveal the presence of such nanostructures.

As evidenced in [6, 24-26] large improvements in the reducibility of ceria-zirconia oxides submitted to the same SRMO-SRSO-SRMO treatments are related with the formation of a pyrochlore type superstructure phase. Complete transformation of ceria-zirconia solid solutions, in which both metallic elements are disordered within the cationic lattice, into the totally ordered pyrochlore requires temperatures as high as 1300ºC in the case of mixed oxides consisting of micron sized crystallites.[33] Nevertheless, it seems quite reasonable that such transformation completes at much lower temperatures when the

mixed oxide phase is in the form of subnanometer thick bi-layer structures, as it is the case of the CYSZ-3C catalyst.

Figure 8 illustrates the spatial distribution of Ce, Zr and Y in the CYSZ-3C catalyst after being submitted to the mildest redox aging protocol used in this study, i.e. SRSO at 950ºC. Note that in spite of the oxidation at high temperature, Ce remains concentrated at the surface as quite thin nanostructures, Figures 8(b) and (c). This is more directly observed on the intensity profiles of the different elements recorded along the paths marked on Figures 8(b) and shown in Figures 8(d) and (e), respectively.

In spite of remaining at surface positions, previous studies on bulk ceria-zirconia oxides have proved that this type of treatment drives an order-disorder transition that destroys the pyrochlore superstructure.[25] This could possibly explain the occurrence of a quite sharp reduction peak in this material, Figure 2(b), at a temperature higher than that of the CYSZ-3C sample. In the latter, the ceria-zirconia structures reside also at the surface but as an Ce-Zr ordered pyrochlore type phase.

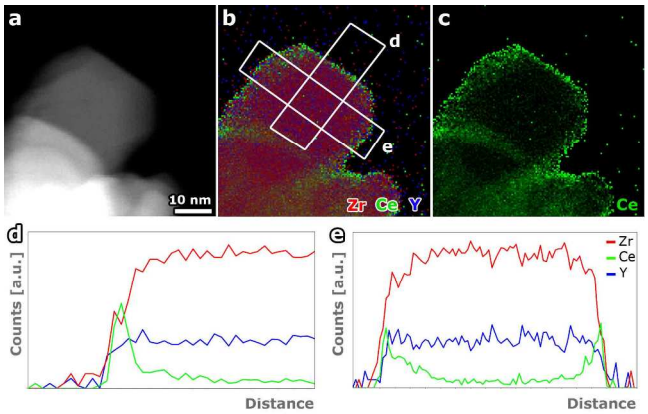

Figure 8. (a) HAADF-STEM image of a CeYSZ-3C sample submitted to a SRSO (950ºC) treatment. (b) XEDS map showing the presence of Zr, Ce and Y, from Ce XEDS map is shown in (c). Line profiles obtained through the particle (d,e) suggest that Ce is present as a layer around the nanostructure.

Increasing the temperature of the oxidizing step of the SRSO treatment up to 1000ºC, for 10h, induces some changes in the spatial distribution of Ce, as shown in Figure 9. In this case, Figure 9(a) shows a HAADF-STEM image of a particle of the catalyst after this treatment. It is clear that the particle morphology is not so well defined. In the elemental distribution of Ce and Zr by XEDS map, Figure 9(b), Ce is still observed to cover the surface of the crystallite but, as suggested by the Ce-XEDS map in Figures 9(c), it is clear that now Ce diffuses in a limited extent into the nanoparticle volume. This is more directly observed on the intensity profiles of the different elements recorded along the paths marked on Figures 9(b) and shown in Figures 9(d) and (e), respectively. The thickness of the cerium-containing layer observed in these profiles is only of a few nanometers. The accumulation of cerium still in positions close to the surface may explain the small difference of OSC with respect to the sample treated at 950ºC for 10 h, Figure 3, and the reversibility observed in the H_2-TPR after the ulterior SRMO step, Figure 2.

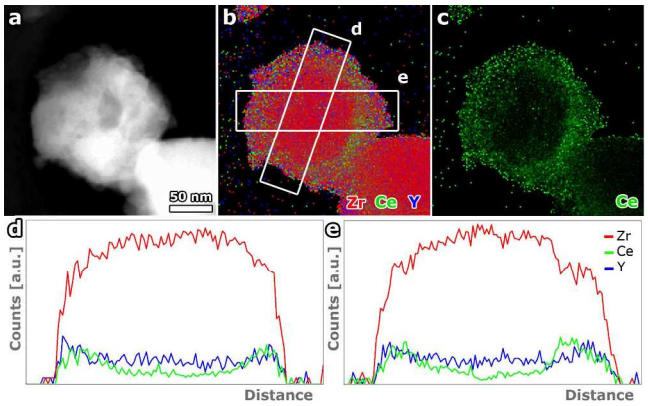

Figure 9. HAADF (a) and XEDS maps (b,c) of the CeYSZ-3C sample submitted to a SRSO (SO at 1000ºC, 10 h). Line profiles obtained through the particle (d,e) show the presence of Ce on the surface and the on-set of Ce diffusion into the bulk of the oxide nanoparticles.

The extent of Ce diffusion into the bulk of the YSZ crystallites changes dramatically after the SRSO 1100ºC-10 h treatment, (see Figure 10). In this case, the results of the STEM-XEDS experiments show an important distinct feature: Ce has completely diffused into the bulk of the YSZ crystallites, depicting an homogeneous distribution throughout the mass of the sample. This is clearly observed in the XEDS maps shown in Figures 10(b) and 10(c), as well as in the intensity profiles of the different elements shown in Figures 10(d) and 10(e). Note how Ce covers now the entire volume of the nanoparticles.

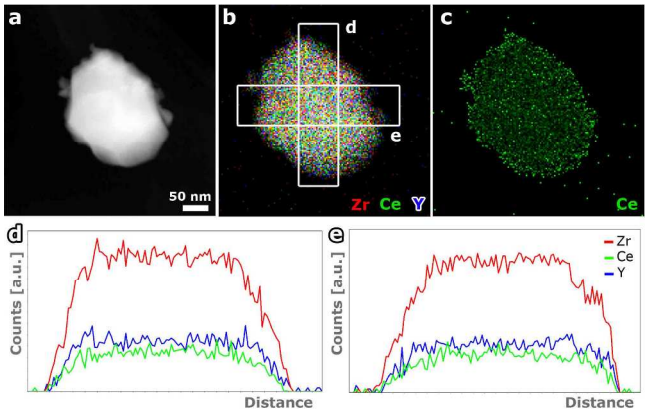

Figure 10. (a) HAADF-STEM image of a CeYSZ-3C sample submitted to a SRSO (1100ºC, 10 h) treatment. (b) XEDS map showing the presence of Zr, Ce and Y, from Ce XEDS map is shown in (c). Line profiles through the particle (d,e) suggest that Ce distributes homogeneously throughout the oxide nanoparticle.

Further evidence is provided in Figure 11, which compares the quantification of STEM-XEDS studies performed on the CYSZ-3C SRSO 950-1h and CYSZ-3C SRSO 1100-10h catalysts. The experiments consisted in this case in acquiring XEDS spectra along lines crossing the catalyst particles from the surface into the bulk, as marked on Figures 11(a) and (c). The results of the quantification of Ce, Zr and Y along the selected paths are plotted in Figures 11(b) and(d).

In the case of the sample treated at 950ºC, Ce signal shows clear peaks at surface locations, on both sides of the catalyst crystallite, with concentrations in the order of 20% mol at surface and below 5% in bulk positions, which is a reasonable

value considering the thickness of the YSZ crystallite in this image. A full, uniform coverage of all the YSZ is not expected since the average, macroscopic, composition of the catalyst is 13% mol Ce. In any case this is not strange, given the large heterogeneity of nanopowder type materials.

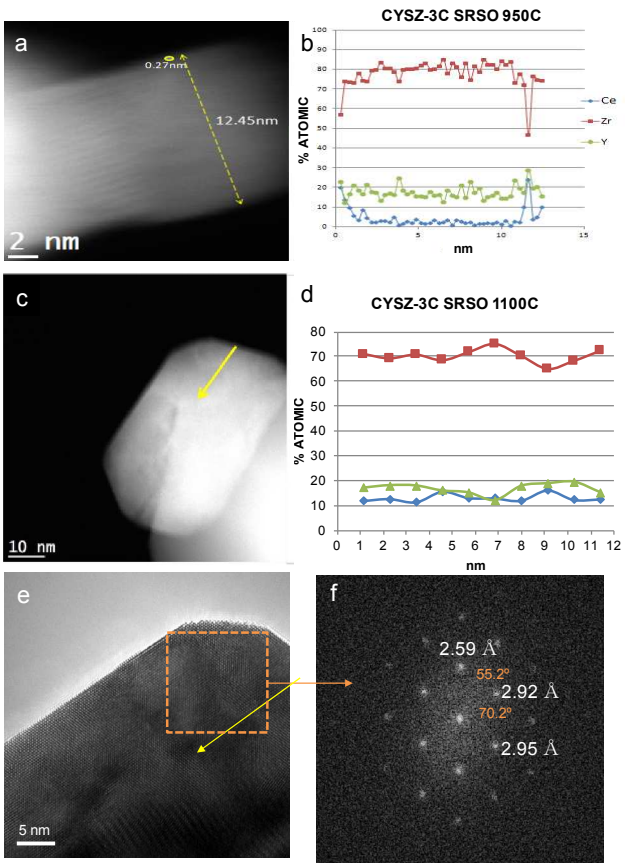

Figure 11. HAADF-STEM images recorded on the CYSZ-3C catalyst after SRSO at (a) 950ºC 1h and (c) 1100ºC -10h, together with their quantification by lineprofiles (b,d) of Ce, Zr and Y from the XEDS spectra along the paths marked in yellow arrow on their corresponding HAADF images. (e) HREM image of the crystal analyzed in (c,d) from which a nanostructural analysis is performed over a selected are by means of its corresponding Digital Diffraction Pattern shown in (f).

In contrast, in the catalyst treated at 1100ºC for 10 h the Ce intensity profile appears uniform throughout the path, with an average Ce composition in the order of 10% mol, i.e. close to the nominal value of 13%. It becomes clear therefore, from the comparison of the two sets of concentration profiles that increasing the oxidation temperature in the SRSO treatment up to 1100ºC allows, as expected, a more efficient diffusion of Ce inside the YSZ crystallites. This homogenization of the Ce distribution must be responsible of both the deterioration of the reducibility of the CYSZ-3C catalyst and the lack of reversibility in the redox response after the additional SRMO treatment. Moreover, the nanostructural analysis performed by HREM, Figure 11(e), confirms that the incorporation of Ce to the original tetragonal YSZ support, lead to the stabilization of a cubic Ce-doped YSZ phase, as clearly suggests the crystallographic results obtained from the analysis of Digital Diffractions Patterns, Figure 11(f). Angles and *d*-spacings measured for the reflections observed in these DDPs are unequivocally indexed as cubic, while no reflections from a tetragonal phase are detected, in good agreement with XRD data, where the c_t/a_t ratio for this sample is very close to $\sqrt{2}$, as expected for a cubic phase, see Table S2 in the Supporting Information".

It seems reasonable that once an uniform, solid-solution type, material has been formed, any further treatment at high temperature may reverse the situation to a surface type phase like the one existing in the original CYSZ-3C catalyst, which is not fully but largely maintained after the SRSO treatments at lower temperatures.

To obtain a macroscopic view of the extent of the diffusion process, XPS analysis was performed on the different samples after SRSO treatments. Table 2 gathers the evolution of the Ce/Zr ratios, as calculated taking into account both the Ce(3d), Ce(4d) and Zr(3d) signals. Note how the initial values, close to 0.25. This ratio is above that expected for the nominal composition of the catalyst (Ce/Zr molar ratio=0.18), which clearly means that Ce is accumulated at surface positions. Note also how this value does not modify during the SRSO treatments when the oxidation is performed up to 1000ºC, for 10h. Only when the oxidation temperature raises up to 1100 a decrease in the ratio is observed, which now comes to values close to the expected, nominal, average (0,18). Therefore, surface chemical analysis by XPS strongly support the observations made by STEM analysis.

Table 2. Ce/Zr ratios at the surface as determined by XPS

CATALYST	Ce/Zr	% mol. Ce
CYSZ-3C SRSO (950ºC 1h)	0,25	20,2
CYSZ-3C SRSO (950ºC 10h)	0,26	20,4
CYSZ-3C SRSO (1000ºC 10h)	0,23	19,0
CYSZ-3C SRSO (1100ºC 10h)	0,17	14,8

CONCLUSIONS

The CYSZ-3C catalyst investigated in this work does not only depict outstanding oxygen exchange capabilities, both in terms of reducibility under H_2 and of OSC, particularly at low temperatures, but also a remarkable resistance against deactivation under high temperature conditions. A reversible change between low reducibility and high reducibility states is observed upon redox cycling. Such reversibility is maintained whenever the maximum temperature remains below 1100ºC, which is in fact a quite meaningful value in relation to the actual conditions during TWC operation.[34]

The combination of advanced STEM-XEDS techniques has proven key to rationalize the origin of such outstanding redox properties. Particularly, STEM-XEDS analysis has revealed as a requirement to detect the nanostructures into which the lanthanide component incorporates and to discriminate them from the underlying YSZ support. Thus from an initial nanostructure in which the supported CeO_2 phase is present as 3D nanoparticles epitaxially grown onto the YSZ surfaces, extended pyrochlore-type bilayers mixing Ce, Zr and Y are formed upon the SRMO-SRSO-SRMO treatment leading to the material that features the best oxygen handling capabilities. It seems that textural changes on the support favoring the exposure of $\{111\}_c$ facets promotes wetting by the Ce-containing phase. Both the 3D nanoparticles and, especially, the bilayers could

only be unambiguously detected from the STEM-XEDS analysis.

Likewise, STEM analysis of the materials resulting from redox SRSO cycling at increasing temperatures has evidenced that Ce remains at surface locations as long as the oxidation temperatures during the SO step does not exceed 1000ºC. The set of XEDS data obtained on the cycled catalysts illustrate the large potential of this type of studies in the investigation of materials chemistry at the nanoscale, in particular of diffusion processes, which is also a quite remarkable result from this investigation.

XEDS line-profiles through the reconstructed volumes of the Ce and Zr signals, evidence that upon oxidation at 1100ºC, the surface of the catalyst nanoparticles becomes Zr-rich whereas Ce has totally diffused into the bulk of the catalyst particles. XPS data confirm, at macroscopic level, the transition from a Ce-enriched surface to a solid-solution situation. Mixing of Ce, Zr and Y at atomic scale throughout the entire bulk of the catalyst nanoparticles precludes the recovery of reducibility of the CYSZ-3C SRSO-1100ºC-10h catalyst upon further SRMO treatment.

The present work sheds also some light onto possible strategies to design novel ceria-zirconia materials. First, it becomes clear that changes increasing the diffusion barrier effect of the support should lead to further improvements in the resistance against redox aging of the supported pyrochlore phase. Such modification would be desirable as long as the intrinsic oxygen handling capabilities of the supported pyrochlore are not negatively affected.

It also becomes clear that it would be desirable finding routes to reach and rebuild the pyrochlore state upon less severe reduction treatments; below 900ºC. This would allow retaining better textural properties of the supported phase. At this respect two factors appear important; first the presence of a support mainly constituted by $\{111\}_c$ facets and, second, finding means to facilitate ordering between Ce and Zr into the pyrochlore superstructure. Both the use of morphologically controlled nano-oxides and the choice of more convenient Ce precursor appear as possible ways for a further insight into these questions.

Finally, and recovering concepts previously proposed for conventional ceria-zirconia materials, the use of the diffusion barrier approach by mixing with nano-alumina constitutes an interesting route to be explored but now on the basis of CYSZ as starting material.

ASSOCIATED CONTENT

Supporting Information

The Supporting Information is available free of charge on the ACS Publications website.

Ultimate OSC Measurements; Tetragonal-phase cell parameters derived from XRD; Pictorial description of the different steps involved in the high temperature aging treatments.

AUTHOR INFORMATION

Corresponding Author

* Prof José J. Calvino

Departamento de Ciencia de los Materiales e Ingeniería Metalúrgica y Química Inorgánica. Facultad de Ciencias, Universidad de Cádiz. Campus Rio San Pedro, Puerto Real, E11510-Cádiz, Spain. jose.calvino@uca.es

Author Contributions

The manuscript was written through contributions of all authors. All authors have given approval to the final version of the manuscript.

ACKNOWLEDGMENT

Financial support from MINECO/FEDER (Project Ref: MAT2013-40823-R), Junta de Andalucía (FQM334 and FQM110) and EU FP7 (ESTEEM2) are acknowledged. J.C.H.-G. acknowledges support from the Ramón y Cajal Fellowships Program of MINECO (RYC-2012-10004).

ABBREVIATIONS

TPR, Temperature Programmed Reduction; OSC, Oxygen Storage Capacity; XRD, X-Ray Diffraction; HRTEM, High Resolution Electron Microscopy; STEM, Scanning Transmission Electron Microscopy; HAADF, High Angle Annular Dark Field; XEDS, X-Ray Energy Dispersive Spectroscopy; EELS, Electron Energy Loss Spectroscopy.

REFERENCES

(1) Fornasiero, P.; Dimonte, R.; Rao, G. R.; Kaspar, J.; Meriani, S.; Trovarelli, A.; Graziani, M., Rh-Loaded CeO_2-ZrO_2 Solid-Solutions as Highly Efficient Oxygen Exchangers - Dependence of the Reduction Behavior and the Oxygen Storage Capacity on the Structural-Properties. *J. Catal.* **1995,** 151, 168-177.
(2) Trovarelli, A.; Fornasiero, P., *Catalysis by Ceria and Related Materials*. Imperial College Press: 2013.
(3) Gandhi, H. S.; Piken, A. G.; Shelef, M.; Delosh, R. G., Laboratory Evaluation of Three-Way Catalysts. SAE International: 1976.
(4) Montini, T.; Melchionna, M.; Monai, M.; Fornasiero, P., Fundamentals and Catalytic Applications of CeO_2-Based Materials. *Chem. Rev.* **2016,** 116, 5987-6041.
(5) Capdevila-Cortada, M.; Vilé, G.; Teschner, D.; Pérez-Ramírez, J.; López, N., Reactivity descriptors for ceria in catalysis. *Appl. Catal. B-Environ.* **2016,** 197, 299-312.
(6) Wang, H.-F.; Guo, Y.-L.; Lu, G.-Z.; Hu, P., Maximizing the Localized Relaxation: The Origin of the Outstanding Oxygen Storage Capacity of κ-$Ce_2Zr_2O_8$. *Angew. Chem. Int. Edit.* **2009,** 48, 8289-8292.
(7) Report on critical raw materials for the EU. In *Report of the Ad hoc Working Group on defining critical raw materials*, 2014; p 1819503.
(8) Abe, H. Current Status and Future of the Car Exhaust Catalyst *Science & Technology Trends Quarterly Review* [Online], 2011, p. 21-31.
(9) Collins, N. R.; Twigg, M. V., Three-way catalyst emissions control technologies for spark-ignition engines—recent trends and future developments. *Top. Catal.* **2007,** 42, 323-332.
(10) Morikawa, A.; Suzuki, T.; Kanazawa, T.; Kikuta, K.; Suda, A.; Shinjo, H., A new concept in high performance ceria–zirconia oxygen storage capacity material with Al2O3 as a diffusion barrier. *Appl. Catal. B-Environ.* **2008,** 78, 210-221.
(11) Christou, S. Y.; Bradshaw, H.; Butler, C.; Darab, J.; Efstathiou, A. M., Effect of Thermal Aging on the Transient Kinetics of Oxygen Storage and Release of Commercial $Ce_xZr_{1-x}O_2$-based Solids. *Top. Catal.* **2009,** 52, 2013 - 2018.
(12) Li, J.; Liu, X.; Zhan, W.; Guo, Y.; Guo, Y.; Lu, G., Preparation of high oxygen storage capacity and thermally stable ceria-zirconia solid solution. *Catal. Sci. Technol.* **2016,** 6, 897-907.
(13) Wu, X.; Yang, B.; Weng, D., Effect of Ce–Zr mixed oxides on the thermal stability of transition aluminas at elevated temperature. *J. Alloy. Compd.* **2004,** 376, 241-245.

(14) Morikawa, A.; Kikuta, K.; Suda, A.; Shinjo, H., Enhancement of oxygen storage capacity by reductive treatment of Al2O3 and CeO2–ZrO2 solid solution nanocomposite. *Appl. Catal. B-Environ.* **2009,** 88, 542-549.
(15) Di Monte, R.; Fornasiero, P.; Kaspar, J.; Graziani, M.; Gatica, J. M.; Bernal, S.; Gomez-Herrero, A., Stabilisation of nanostructured $Ce_{0.2}Zr_{0.8}O_2$ solid solution by impregnation on Al_2O_3: a suitable method for the production of thermally stable oxygen storage/release promoters for three-way catalysts. *Chem. Commun.* **2000**, 2167-2168.
(16) Lan, L.; Chen, S.; Cao, Y.; Zhao, M.; Gong, M.; Chen, Y., Preparation of ceria–zirconia by modified coprecipitation method and its supported Pd-only three-way catalyst. *J. Colloid. Interf. Sci.* **2015,** 450, 404-416.
(17) Dong, Q.; Yin, S.; Guo, C.; Sato, T., $Ce_{0.5}Zr_{0.4}Sn_{0.1}O_2/Al_2O_3$ catalysts with enhanced oxygen storage capacity and high CO oxidation activity. *Catal. Sci. Technol.* **2012,** 2, 2521-2524.
(18) Yang, P.; Yang, S.; Shi, Z.; Tao, F.; Guo, X.; Zhou, R., Accelerating effect of ZrO_2 doping on catalytic performance and thermal stability of CeO_2–CrO_x mixed oxide for 1,2-dichloroethane elimination. *Chem. Eng. J.* **2016,** 285, 544-553.
(19) Kanazawa, T.; Suzuki, J.; Takada, T.; Suzuki, T.; Morikawa, A.; Suda, A.; Sobukawa, H.; Sugiura, M., Development of Three-way Catalyst Using Composite Alumina-Ceria-Zirconia. SAE International: 2003.
(20) Tinoco, M.; Sanchez, J. J.; Yeste, M. P.; Lopez-Haro, M.; Trasobares, S.; Hungria, A. B.; Bayle-Guillemaud, P.; Blanco, G.; Pintado, J. M.; Calvino, J. J., Low-Lanthanide-Content CeO_2/MgO Catalysts with Outstandingly Stable Oxygen Storage Capacities: An In-Depth Structural Characterization by Advanced STEM Techniques. *Chemcatchem* **2015,** 7, 3763-3778.
(21) Masui, T.; Nakano, K.; Ozaki, T.; Adachi, G.-y.; Kang, Z.; Eyring, L., Redox Behavior of Ceria−Zirconia Solid Solutions Modified by the Chemical Filing Process. *Chem. Mater.* **2001,** 13, 1834-1840.
(22) Yeste, M. P.; Hernandez-Garrido, J. C.; Arias, D. C.; Blanco, G.; Rodriguez-Izquierdo, J. M.; Pintado, J. M.; Bernal, S.; Perez-Omil, J. A.; Calvino, J. J., Rational design of nanostructured, noble metal free, ceria-zirconia catalysts with outstanding low temperature oxygen storage capacity. *J. Mater .Chem. A* **2013,** 1, 4836-4844.
(23) Kašpar, J.; Di Monte, R.; Fornasiero, P.; Graziani, M.; Bradshaw, H.; Norman, C., Dependency of the Oxygen Storage Capacity in Zirconia–Ceria Solid Solutions upon Textural Properties. *Top. Catal.* **2001,** 16, 83-87.
(24) Baker, R. T.; Bernal, S.; Blanco, G.; Cordon, A. M.; Pintado, J. M.; Rodriguez-Izquierdo, J. M.; Fally, F.; Perrichon, V., Reversible changes in the redox behaviour of a $Ce_{0.68}Zr_{0.32}O_2$ mixed oxide: effect of alternating the re-oxidation temperature after reduction at 1223 K. *Chem. Commun.* **1999**, 149-150.
(25) Yeste, M. P.; Hernandez, J. C.; Trasobares, S.; Bernal, S.; Blanco, G.; Calvino, J. J.; Perez-Omil, J. A.; Pintado, J. M., First stage of thermal aging under oxidizing conditions of a Ce(0.62)Zr(0.38)O(2) mixed oxide with an ordered cationic sublattice: A chemical, nanostructural, and nanoanalytical study. *Chem. Mater.* **2008,** 20, 5107-5113.
(26) Bernal, S.; Blanco, G.; Calvino, J. J.; Hernandez, J. C.; Perez-Omil, J. A.; Pintado, J. M.; Yeste, M. R., Some recent results on the correlation of nano-structural and redox properties in ceria-zirconia mixed oxides. *J. Alloy. Compd.* **2008,** 451, 521-525.
(27) Hernandez, J. C.; Hungria, A. B.; Perez-Omil, J. A.; Trasobares, S.; Bernal, S.; Midgley, P. A.; Alavi, A.; Calvino, J. J., Structural surface investigations of cerium-zirconium mixed oxide nanocrystals with enhanced reducibility. *J. Phys. Chem. C* **2007,** 111, 9001-9004.
(28) Montini, T.; Banares, M. A.; Hickey, N.; Di Monte, R.; Fornasiero, P.; Kaspar, J.; Graziani, M., Promotion of reduction in $Ce_{0.5}Zr_{0.5}O_2$: the pyrochlore structure as effect rather than cause? *Phys. Chem. Chem. Phys.* **2004,** 6, 1-3.
(29) Montini, T.; Hickey, N.; Fornasiero, P.; Graziani, M.; Bañares, M. A.; Martinez-Huerta, M. V.; Alessandri, I.; Depero, L. E., Variations in the Extent of Pyrochlore-Type Cation Ordering in $Ce_2Zr_2O_8$: A t'−κ Pathway to Low-Temperature Reduction. *Chem. Mater.* **2005,** 17, 1157-1166.
(30) Allen, L. J.; D'Alfonso, A. J.; Freitag, B.; Klenov, D. O., Chemical mapping at atomic resolution using energy-dispersive x-ray spectroscopy. *MRS Bulletin* **2012,** 37, 47-52.
(31) Cies, J. M.; del Rio, E.; Lopez-Haro, M.; Delgado, J. J.; Blanco, G.; Collins, S.; Calvino, J. J.; Bernal, S., Fully Reversible Metal Deactivation Effects in Gold/Ceria-Zirconia Catalysts: Role of the Redox State of the Support. *Angew. Chem. Int. Edit.* **2010,** 49, 9744-9748.
(32) Gonzalez, J. C.; Hernandez, J. C.; Lopez-Haro, M.; del Rio, E.; Delgado, J. J.; Hungria, A. B.; Trasobares, S.; Bernal, S.; Midgley, P. A.; Calvino, J. J., 3D Characterization of Gold Nanoparticles Supported on Heavy Metal Oxide Catalysts by HAADF-STEM Electron Tomography. *Angew. Chem. Int. Edit.* **2009,** 48, 5313-5315.
(33) Kishimoto, H.; Omata, T.; Otsuka-Yao-Matsuo, S.; Ueda, K.; Hosono, H.; Kawazoe, H., Crystal structure of metastable K-CeZrO4 phase possessing an ordered arrangement of Ce and Zr ions. *J. Alloy. Compd.* **2000,** 312, 94-103.
(34) Gutierrez Ortiz, M. A.; Botas Echevarría, J. A.; Gonzalez-Velasco, J. R.; Gonzalez Marcos, M. P., Catalysis, automobile and environment. *An. Real. Soc. Esp. Quim.* **2002**, 24-35.

TOC (Table Of Content graphic)